

Extended Dark Matter EFT

Tommi Alanne* and Florian Goertz†

Max-Planck-Institut für Kernphysik, Saupfercheckweg 1, 69117 Heidelberg, Germany

Conventional approaches to describe dark matter phenomenology at collider and (in)direct detection experiments in the form of dark matter effective field theory or simplified models suffer in general from drawbacks regarding validity at high energies and/or generality, limiting their applicability. In order to avoid these shortcomings, we propose a hybrid framework in the form of an effective theory, including, however, both the dark matter states and a mediator connecting the former to the Standard Model fields. Since the mediation can be realized through rather light new dynamical fields allowing for non-negligible collider signals in missing energy searches, the framework remains valid for the phenomenologically interesting parameter region, while retaining correlations dictated by gauge symmetry. Moreover, a richer new-physics sector can be consistently included via higher-dimensional operators. Interestingly, for fermionic and scalar dark matter with a (pseudo-)scalar mediator, the leading effects originate from dimension-five operators, allowing to capture them with a rather small set of new couplings. We finally examine the correlations between constraints from reproducing the correct relic density, direct-detection experiments, and mono-jet and Higgs + missing energy signatures at the LHC.

I. INTRODUCTION AND SETUP

The origin of the dark matter (DM) observed in the universe is one of the biggest mysteries in physics. A multitude of experiments, which are probing very diverse energies, are currently running or in preparation to address this question. Experiments aiming for a direct detection of DM particles via nuclear recoil typically probe collision energies in the keV range, while collider experiments, trying to produce DM particles, feature momentum transfers exceeding the TeV scale.

Combining the results from all kinds of experiments in a single, consistent, yet general framework is important in order to resolve the nature of DM. Bounds from direct detection experiments are usually interpreted in an effective field theory (EFT) approach, removing the mediator that couples the DM particles to the Standard Model (SM) as an explicit dynamical degree of freedom at low energies. This is possible, if the mediator is assumed to be much heavier than the scale of the experiments, and its effects can thus be described by generic EFT operators, consisting only of the SM and DM fields.

On the other hand, collider experiments such as the LHC run at much larger energies, and it turns out that the momentum transfers lie typically at (or above) interesting mass ranges for the mediator, to which the analyses are sensitive (unless the model is very strongly coupled [1]). Thus, the EFT description becomes invalid since the mediator is missing in the spectrum [2, 3]. In consequence, collider searches are typically interpreted in terms of simplified models where the mediator is not removed, and its interactions with the SM and the DM are simply parametrized by $D \leq 4$ operators. For the sake of flexibility, the simplest implementations do not

require gauge-invariance and are thus not well behaved at large energies. A further drawback of this approach is that they are still specific models that do not allow for a maximally general description of the dark sector. In the end, one suffers either from a lack of generality or, even worse, from a lack of validity.

In this article, we want to propose a hybrid framework, which can alleviate the above problems: We will consider the minimal amount of additional *dynamical* degrees of freedom—a DM particle *and* a mediator—which is able to generate the correct DM abundance and allows for testability at TeV scale energies, while retaining the generality and consistency of the EFT framework.

We will, thus, consider the SM extended by a SM-singlet particle, \mathcal{D} , that is stable on cosmological scales, and a mediator, \mathcal{M} , that couples it to the SM, as well as higher-dimensional EFT operators, consisting of these fields. We will start by assuming the DM to be a fermion, $\mathcal{D} = \chi$, and the mediator a (pseudo)scalar, $\mathcal{M} = \mathcal{S}(\tilde{\mathcal{S}})$, and then move on to consider also the case of scalar DM. In these setups, the leading EFT effects will be at the level of $D = 5$ operators, and their inclusion allows to parametrize physics of the dark sector beyond the single DM particle and the mediator.¹

In fact, while the inclusion of the latter particles makes the theory valid at collider energies, the augmentation with $D = 5$ operators accounts for the fact that the dark/new sector is likely to be non-minimal. Indeed, there is no stringent reason to believe that the sector related with the DM consists only of very few particles, while the SM has a very rich structure. On the other hand, it is conceivable that a few of the new particles (the DM particle and the mediator) are considerably lighter

* tommi.alanne@mpi-hd.mpg.de

† florian.goertz@mpi-hd.mpg.de

¹ The generalization to (fermionic or scalar) DM with a vector mediator calls for the inclusion of $D = 6$ operators and a study of the very rich phenomenology, and we will leave this for future work.

than the rest of the new physics (NP). For example, the mediator could be a (pseudo-)Goldstone boson of a spontaneously broken global symmetry. The goal of this article is to provide the theoretical framework of this extended DM EFT (eDMEFT) approach, demonstrating its strength in phenomenological analyses, as well as pointing out emerging synergies and generic correlations between observables, which are retained in the EFT approach.

A. Fermionic DM with a scalar or pseudoscalar mediator

The effective Lagrangian of the model described above, with a fermion singlet, χ , and a (CP even) scalar, \mathcal{S} , including operators up to $D = 5$ (following normalisations of Ref. [4]) reads²

$$\begin{aligned} \mathcal{L}_{\text{eff}}^{\mathcal{S}\chi} = & \mathcal{L}_{\text{SM}} + \frac{1}{2} \partial_\mu \mathcal{S} \partial^\mu \mathcal{S} - \frac{1}{2} \mu_S^2 \mathcal{S}^2 + \bar{\chi} i \not{\partial} \chi - m_\chi \bar{\chi} \chi \\ & - \lambda'_{S1} v^3 \mathcal{S} - \frac{\lambda'_S}{2\sqrt{2}} v \mathcal{S}^3 - \frac{\lambda_S}{4} \mathcal{S}^4 \\ & - \lambda'_{HS} v |H|^2 \mathcal{S} - \lambda_{HS} |H|^2 \mathcal{S}^2 \\ & - y_S \mathcal{S} \bar{\chi}_L \chi_R + \text{h.c.} \\ & - \frac{\mathcal{S}}{\Lambda} [c_{\lambda S} \mathcal{S}^4 + c_{HS} |H|^2 \mathcal{S}^2 + c_{\lambda H} |H|^4] \\ & - \frac{\mathcal{S}}{\Lambda} \left[(y_d^S)^{ij} \bar{Q}_L^i H d_R^j + (y_u^S)^{ij} \bar{Q}_L^i \tilde{H} u_R^j \right. \\ & \quad \left. + (y_\ell^S)^{ij} \bar{L}_L^i H \ell_R^j + \text{h.c.} \right] \\ & - \frac{y_S^{(2)} \mathcal{S}^2 + y_H^{(2)} |H|^2}{\Lambda} \bar{\chi}_L \chi_R + \text{h.c.} \\ & - \frac{\mathcal{S}}{\Lambda} \frac{1}{16\pi^2} \left[g'^2 c_B^S B_{\mu\nu} B^{\mu\nu} + g^2 c_W^S W_{\mu\nu}^I W^{\mu\nu I} \right. \\ & \quad \left. + g_s^2 c_G^S G^{a\mu\nu} G_{\mu\nu}^a \right]. \end{aligned} \quad (1)$$

Here Q_L^i and L_L^i are the i -th generation left-handed $\text{SU}(2)_L$ quark and lepton doublets, resp., d_R^j , u_R^j , and ℓ_R^j are the right-handed singlets for generation j , and H is the Higgs doublet. The Higgs doublet develops a vacuum expectation value (vev), $|\langle H \rangle| \equiv v/\sqrt{2} \simeq 174$ GeV, triggering electroweak symmetry breaking (EWSB). In unitary gauge, the Higgs field is expanded around the vev as $H \simeq 1/\sqrt{2}(0, v + h)^T$. Here, h is the physical Higgs boson, with mass $m_h \approx 125$ GeV. We assume that the mediator does not develop a vev and have, thus, included a linear term in \mathcal{S} .

Besides the SM couplings, there are several new interactions, both at the renormalizable ($D = 4$) level and

in the form of effective $D = 5$ operators. In the scalar sector, the cubic and quartic terms in the singlet potential are parametrized by the couplings λ'_S and λ_S , resp., while the Higgs-portal couplings involving one or two singlets are denoted by λ'_{HS} and λ_{HS} , resp. Note that, after EWSB, the latter coupling provides a contribution to the mediator mass, which is given by

$$m_S = \sqrt{\mu_S^2 + \lambda_{HS} v^2}. \quad (2)$$

In addition, there is a Yukawa coupling between the scalar mediator, \mathcal{S} , and the DM fermions, χ , denoted by y_S . At the $D = 5$ level, all interactions are suppressed by one power of the scale of heavy NP, Λ , which mediates contact interactions between the various fields. In the pure scalar sector, gauge invariant terms feature four ($c_{\lambda H}$), two (c_{HS}), or zero ($c_{\lambda S}$) Higgs fields. In order to couple the mediator, \mathcal{S} , to SM fermions, the presence of a Higgs doublet is required, allowing for $D = 5$ Yukawa-like couplings, $\sim (y_d^S)^{ij}, (y_u^S)^{ij}$. Scalar couplings to the DM fermions at the $D = 5$ level, on the other hand, involve either two scalar singlets or two doublets, due to gauge invariance, parametrized by $y_S^{(2)}$ and $y_H^{(2)}$, respectively. Finally, there are effective couplings of \mathcal{S} to the $\text{U}(1)_Y$, $\text{SU}(2)_L$, and $\text{SU}(3)_c$ field strengths squared, denoted by c_B^S , c_W^S , and c_G^S . In the following, we assume the interactions with \mathcal{S} to conserve CP, and thus all coefficients in the Lagrangian of Eq. (1) are real.

We conclude this discussion noting that, if the new sector residing at the scale Λ is governed by a coupling g_* , the effective coefficients above can be assigned a certain scaling in this coupling (see e.g. [7–10]), which in our case (without assuming the Higgs to be a pseudo-Goldstone state) reads $c_{\lambda S} \sim c_{HS} \sim c_{\lambda H} \sim g_*^3$, $y_f^S \sim y_f g_*$, $y_{S,H}^{(2)} \sim g_*^2$, $c_V^S \sim g_*$. This allows to order the operators according to their expected importance in a certain coupling regime and can for example be used to reduce the number of $D = 6$ operators to be considered to leading approximation in the case of a vector mediator.³

The eDMEFT Lagrangian, Eq.(1), allows to describe phenomena relevant for collider searches for DM as well as for direct (and indirect) detection experiments, as we will now explore in more detail. For example, for a non-negligible $(y_q^S)^{ij}/\Lambda$, the operators $\mathcal{S} \bar{Q}_L^i H q_R^j$ can mediate interactions of DM with a nucleus, coupling the mediator to the DM via the $\mathcal{S} \bar{\chi} \chi$ interaction, see the upper panel of Fig. 1, where the scalar mediator is depicted by double-dashed lines, while the fermionic DM is represented by faint double-lines. The same combination of operators induces, on the other hand, DM signals at the LHC in two different, but correlated, incarnations. Mono-jet and Higgs+missing transverse energy (\cancel{E}_T) signatures are

² The EFT of the SM plus just a scalar singlet \mathcal{S} has been explored in Refs [4–6].

³ As shown recently [11], such a counting could also allow to lift the ambiguity in determining masses of new states in an EFT approach.

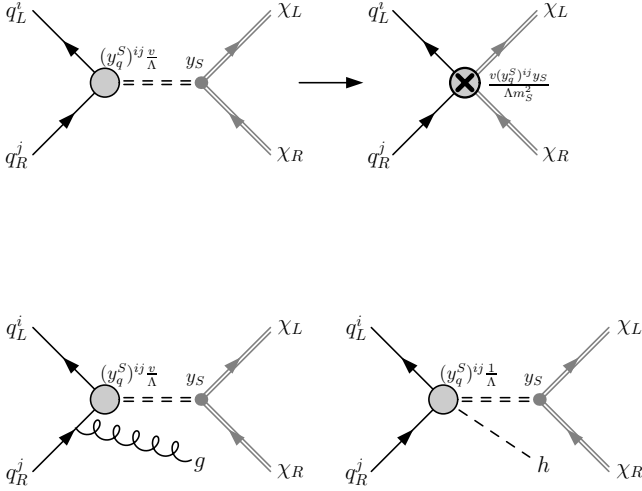


FIG. 1. Relevant diagrams contributing to nuclear interaction with fermionic DM (first row) and corresponding DM observables at hadron colliders (monojet and Higgs+ \cancel{E}_T , second row), turning on the interactions $\sim (y_q^S)^{ij}$ and $\sim y_S$. The diagrams are similar for scalar and pseudo-scalar mediators, where for the latter case, the operator coefficients in Eq. (1) are to be replaced by the corresponding (tilded) coefficients in Eq. (3). See text for details.

generated, radiating off a gluon from the (initial state) quarks and considering the physical Higgs within H in the $S\bar{Q}_L^i H q_R^j$ operator, resp., while the $S \rightarrow \bar{\chi}\chi$ transition is responsible for the \cancel{E}_T , as shown in the lower panel of Fig. 1.⁴

Note that, since the Yukawa-like couplings $\sim (y_q^S)^{ij}$ can feature flavour-changing neutral currents (FCNCs), a flavour-protection mechanism like minimal flavour violation could be thought of, which would lead to a suppressed coupling to the light valence quarks and thus small effects at colliders at the tree level (see also Ref. [16]). In an agnostic approach, however, all couplings could be treated as free, and some tuning withing the Yukawa structure could be allowed, considering only ‘direct’ experimental constraints allowing, in principle, for considerable effects for valence quarks. Finally note that, in case light-quark contributions were suppressed, the operators could still induce a coupling to gluons at the one-loop level, via heavy-quark triangle diagrams.

If other $D = 5$ operators (as well as the portal coupling, λ'_{HS}) are set to zero for the moment, all three processes above scale in terms of effective coefficients as $y_S (y_q^S)^{ij} / \Lambda$, and we can explore the complementarity and combined information of both types of experiments in one framework. We will examine this in more detail in the

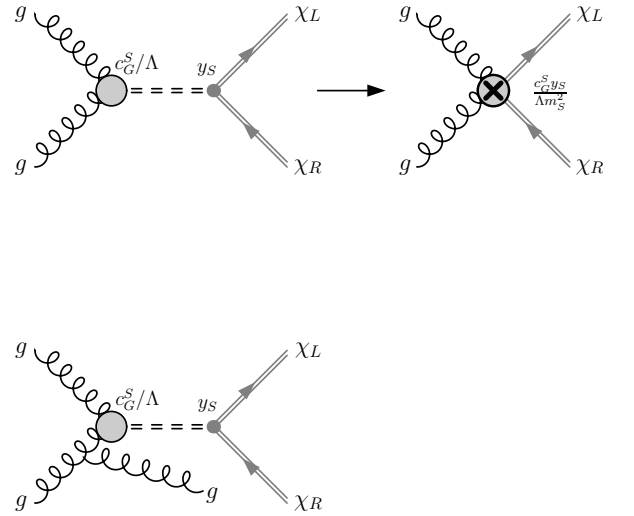


FIG. 2. Relevant diagrams contributing to nuclear interaction with fermionic DM (first row) and corresponding DM observables at hadron colliders (monojet, second row), turning on the interactions $\sim c_G^S$ and $\sim y_S$. The diagrams are similar for pseudo-scalar mediators, employing the corresponding tilded coefficients, as discussed before.

next section. As an alternative option, we will also consider the coupling of the mediator to the proton/nucleus via the $SG^{a\mu\nu}G_{\mu\nu}^a$ operator, trading $(y_q^S)^{ij}$ for c_G^S , which allows for the production of DM in gluon fusion. The corresponding diagrams for the processes discussed above are shown in Fig. 2, where similar correlations can be explored (with the Higgs-associated production now being absent at leading order). In the same context, another interesting opportunity is to produce the mediator in weak-boson fusion (WBF), by turning on c_W^S or c_B^S , as depicted by the diagrams in the last row of Fig. 15 and commented on further below.

On the other hand, the Higgs boson might play a crucial role in coupling the DM to quarks and gluons. First, it can provide a portal to the mediator, via the couplings $\lambda_{HS}, \lambda'_{HS}$, connecting the SM to the dark sector. In particular if the second operator is present, the mediator can be produced in gluon-fusion Higgs production via mixing with the Higgs field connecting then to the DM via y_S . The corresponding diagrams are given in Fig. 3, where again unavoidably the Higgs+ \cancel{E}_T channel is present, fixed by gauge invariance. Finally, the operators in Eq. (1) also allow for interactions of DM with hadrons mediated *directly* by Higgs exchange, if the coefficient $y_H^{(2)}$ is non-vanishing. Turning on this single coupling provides an instantaneous link between the Higgs field and the DM via a contact interaction, inducing all processes discussed before, with the diagrams given in Fig. 4. Once more, the Higgs+ \cancel{E}_T channel is induced by gauge invariance.

Let us conclude this discussion by emphasizing again that the Lagrangian of Eq. (1) allows to consistently com-

⁴ At low (nuclear) energies, we can also integrate out the mediator to arrive at a four-fermion interaction, as considered in the usual DM EFT [12–15]. Now, however, the effective coefficient is fixed by Eq. (1).

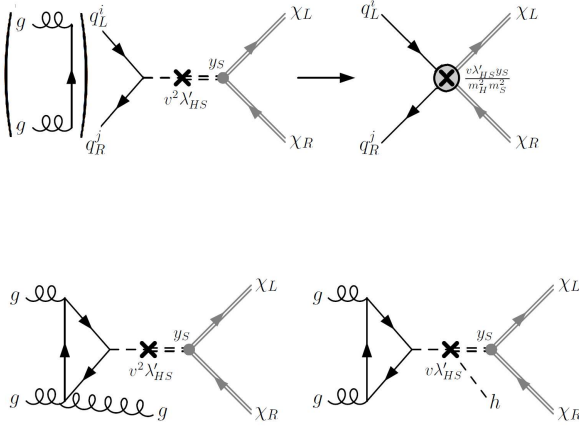


FIG. 3. Relevant diagrams contributing to nuclear interaction with fermionic DM (first row) and corresponding DM observables at hadron colliders (monojet and Higgs+ \cancel{E}_T , second row), turning on the interactions $\sim \lambda'_{HS}$ and $\sim y_S$. Note that the corresponding diagrams are not present for pseudo-scalar mediators, which only appear in pairs.

bine various processes and to include information from different kinds of sources. For example, DM might be produced by a combination of different mechanisms, e.g. via the mediator \mathcal{S} (triggered by $(y_q^S)^{ij}$, c_G^S , or a portal), but also via direct Higgs exchange—due to the effective $y_H^{(2)}$, even without $H - \mathcal{S}$ mixing—where each contribution leads to characteristic correlations between LHC physics and direct (as well as indirect) detection experiments. We note that the direct Higgs couplings also enter in invisible Higgs decays constraining their size, while resonance searches are directly sensitive to the properties of the mediator. The eDMEFT allows to describe and combine all these different phenomena in a general (inclusive) and consistent way including resonance searches for the mediator particle, which would not be possible in a simple DM EFT or a simplified-model approach. Yet, it is simple enough to keep predictivity and to be straightforwardly implemented into tools for automated event generation and implementation of constraints. Finally, matching UV complete models to the eDMEFT will also allow to interpret experimental results obtained in the latter framework in terms of such explicit models, without the need to repeat the analysis for numerous different setups.

Before exploring in more detail the LHC and direct-detection phenomenology in the eDMEFT approach, we will now turn to the remaining scenarios of DM coupled to the SM via a potentially light mediator, which can be analyzed in a similar way. First, we will consider the case of a CP-odd scalar, $\tilde{\mathcal{S}}$, which has several interesting features. On the one hand, direct detection bounds with a CP-odd scalar mediator are much weaker due to mo-

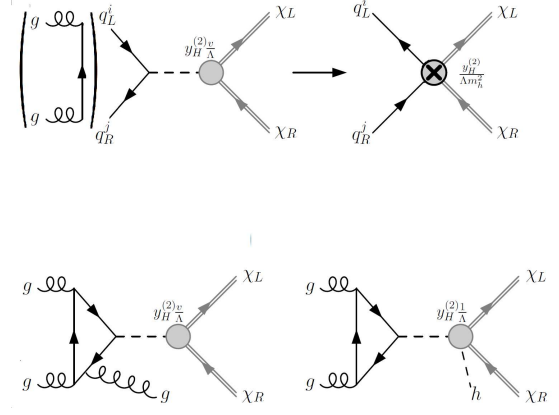


FIG. 4. Relevant diagrams contributing to nuclear interaction with fermionic DM (first row) and corresponding DM observables at hadron colliders (monojet and Higgs+ \cancel{E}_T , second row), turning on the interaction $\sim y_H^{(2)}$.

mentum suppression of the cross section [17, 18]. Moreover, besides the $D = 5$ pure scalar interactions, the portal with a single mediator vanishes, which automatically avoids the mixing between the scalars. The Lagrangian now becomes

$$\begin{aligned} \mathcal{L}_{\text{eff}}^{\tilde{\mathcal{S}}\chi} = & \mathcal{L}_{\text{SM}} + \frac{1}{2} \partial_\mu \tilde{\mathcal{S}} \partial^\mu \tilde{\mathcal{S}} - \frac{1}{2} \mu_{\tilde{\mathcal{S}}}^2 \tilde{\mathcal{S}}^2 + \tilde{\chi} i \not{\partial} \chi - m_\chi \tilde{\chi} \chi \\ & - \frac{\lambda_{\tilde{\mathcal{S}}}}{4} \tilde{\mathcal{S}}^4 - \lambda_{H\tilde{\mathcal{S}}} |H|^2 \tilde{\mathcal{S}}^2 - y_{\tilde{\mathcal{S}}} \tilde{\mathcal{S}} i \tilde{\chi}_L \chi_R + \text{h.c.} \\ & - \frac{\tilde{\mathcal{S}}}{\Lambda} \left[(y_d^{\tilde{\mathcal{S}}})^{ij} i \bar{Q}_L^i H d_R^j + (y_u^{\tilde{\mathcal{S}}})^{ij} i \bar{Q}_L^i \tilde{H} u_R^j \right. \\ & \quad \left. + (y_\ell^{\tilde{\mathcal{S}}})^{ij} i \bar{L}_L^i H \ell_R^j + \text{h.c.} \right] \\ & - \frac{y_{\tilde{\mathcal{S}}}^{(2)} \tilde{\mathcal{S}}^2 + y_H^{(2)} H^\dagger H}{\Lambda} \tilde{\chi}_L \chi_R + \text{h.c.} \\ & - \frac{\tilde{\mathcal{S}}}{\Lambda} \frac{1}{16\pi^2} \left[g'^2 c_B^{\tilde{\mathcal{S}}} B_{\mu\nu} \tilde{B}^{\mu\nu} + g^2 c_W^{\tilde{\mathcal{S}}} W^{I\mu\nu} \tilde{W}_{\mu\nu}^I \right. \\ & \quad \left. + g_s^2 c_G^{\tilde{\mathcal{S}}} G^{a\mu\nu} \tilde{G}_{\mu\nu}^a \right]. \end{aligned} \quad (3)$$

Here, the contact interactions with gauge bosons feature dual field strength tensors, while all terms can be interpreted analogously as in the CP-even scalar case. In particular, the very same discussion as before on generic correlations between different observables can be performed. Note, however, that due to the vanishing single-mediator portal, no production via the Higgs is possible at the level of $D \leq 4$ interactions, which makes the (extended) EFT terms $\sim y_q^{\tilde{\mathcal{S}}}, c_{G,B,W}^{\tilde{\mathcal{S}}}, y_H^{(2)}$ even more interesting. We will again assume no new sources of CP violation, and the coefficients in Lagrangian in Eq. (3) are real.

B. Scalar DM with a scalar mediator

We finally move to the case of (singlet) scalar DM, denoted by $\mathcal{D} = \chi_s$ still considering a scalar mediator, $\mathcal{M} = \mathcal{S}$. The Lagrangian for this setup, at the $D = 5$ level, reads

$$\begin{aligned}
\mathcal{L}_{\text{eff}}^{\mathcal{S}\chi_s} = & \mathcal{L}_{\text{SM}} + \frac{1}{2}\partial_\mu \mathcal{S} \partial^\mu \mathcal{S} + \frac{1}{2}\partial_\mu \chi_s \partial^\mu \chi_s - \lambda'_{S1} v^3 \mathcal{S} \\
& - \frac{1}{2}\mu_S^2 \mathcal{S}^2 - \frac{1}{2}m_{\chi_s}^2 \chi_s^2 - \frac{\lambda'_S}{2\sqrt{2}} v \mathcal{S}^3 - \frac{\lambda_S}{4} \mathcal{S}^4 \\
& - \frac{\lambda_{\chi_s}}{4} \chi_s^4 - \lambda'_{HS} v |H|^2 \mathcal{S} - \lambda_{HS} |H|^2 \mathcal{S}^2 \\
& - \frac{\lambda'_{S\chi_s}}{2\sqrt{2}} v \mathcal{S} \chi_s^2 - \lambda_{S\chi_s} \mathcal{S}^2 \chi_s^2 - \lambda_{H\chi_s} |H|^2 \chi_s^2 \\
& - \frac{\mathcal{S}}{\Lambda} [c_{\lambda S} \mathcal{S}^4 + c_{HS} |H|^2 \mathcal{S}^2 + c_{\lambda H} |H|^4 \\
& + c_{S\chi_s} \mathcal{S}^2 \chi_s^2 + c_{\lambda\chi_s} \chi_s^4 + c_{H\chi_s} |H|^2 \chi_s^2] \\
& - \frac{\mathcal{S}}{\Lambda} \left[(y_d^S)^{ij} \bar{Q}_L^i H d_R^j + (y_u^S)^{ij} \bar{Q}_L^i \tilde{H} u_R^j \right. \\
& \left. + (y_\ell^S)^{ij} \bar{L}_L^i H \ell_R^j + \text{h.c.} \right] \\
& - \frac{\mathcal{S}}{\Lambda} \frac{1}{16\pi^2} \left[g'^2 c_B^S B_{\mu\nu} B^{\mu\nu} + g^2 c_W^S W^{I\mu\nu} W_{\mu\nu}^I \right. \\
& \left. + g_s^2 c_G^S G^{a\mu\nu} G_{\mu\nu}^a \right].
\end{aligned} \tag{4}$$

We assume again that the mediator, \mathcal{S} , does not develop a vev, while a Z_2 symmetry assures stability of χ_s .

For pseudo-scalar, $\mathcal{M} = \tilde{\mathcal{S}}$, the terms in the last two square brackets are replaced similarly as before (Eq. (1) \rightarrow Eq. (3)). However, all further contributions with an odd number of \mathcal{S} are absent, and further dynamics would be required for s -channel mediation between the DM and SM fields, and therefore, we do not consider this scenario here.

Crucial (new) terms in Eq. (4) are the portal-like interactions connecting the DM to the mediator, $\lambda_{S\chi_s}$, $\lambda'_{S\chi_s}$ (and the corresponding $D = 5$ operators, containing odd powers of \mathcal{S} and even powers of χ_s , i.e., the terms $\sim c_{S\chi_s}, c_{\lambda\chi_s}, c_{H\chi_s}$), replacing $y_S/y_{\tilde{S}}$ of the fermionic DM case. Furthermore, there is a new direct $D = 4$ portal to the DM via the Higgs field, given by $\lambda_{H\chi_s}$, instead of the corresponding term $\sim y_H^{(2)}$ for fermionic DM, as well as a quartic DM self-interaction $\sim \lambda_{\chi_s}$. We will discuss the corresponding changes in the processes described above for fermionic dark matter, including the respective diagrams, in the next section.

II. COMPLEMENTARY CONSTRAINTS WITHIN ONE FRAMEWORK: eDMEFT

We will now explore phenomenological aspects of all the models described above, making use of the correlations predicted in our eDMEFT approach, as anticipated

before. In particular, we will address the question of how many events in DM searches at the LHC can be expected, given limits from direct detection experiments, without restricting to an explicit NP model. The presence of the mediator in our EFT will ensure the validity of the analysis for collider searches. We will finally discuss the inclusion of further processes like loop-induced DM production via $D = 5$ operators, invisible Higgs decays, Higgs pair production, as well as resonance searches in the same framework.

As main observables, we consider the direct-detection cross section for the scattering of DM off a nucleus, N ,

$$\sigma_N \equiv \sigma(N\mathcal{D} \rightarrow N\mathcal{D}), \tag{5}$$

and the cross section for a monojet signal at the 13 TeV LHC

$$\sigma_j \equiv \sigma(pp \rightarrow j + \cancel{E}_T). \tag{6}$$

In addition, in the cases where the mediator is produced via the new $D = 5$ operators coupling it to quarks, we expect also the cross section for producing the Higgs in association with missing transverse energy to be comparable to the monojet cross section and consider also

$$\sigma_{h+\cancel{E}_T} \equiv \sigma(pp \rightarrow h + \cancel{E}_T). \tag{7}$$

We can now calculate how many events in LHC DM searches (monojet and Higgs+ \cancel{E}_T) are possible, given the limits from direct detection, in the framework of different eDMEFTs discussed in the last section, each representing a large class of NP models. The LHC results could thus potentially rule out certain DM incarnations very generally or support/constrain them in synergy with direct-detection experiments. In that context, note that the currently most stringent direct detection constraint corresponds to $N = \text{Xe}$ and is given by XENON1T [19].

Going through the different scenarios, we will address this question, always turning on a set of (one or two) NP couplings that allow for a different production mechanism of the DM or different DM–nucleus interaction, considering quark- and gluon-induced production, production through the Higgs-mediator portal, and production through direct Higgs–DM interactions.

The requirement to generate the correct relic abundance implies further constraints on the same operators that are entering DM–SM scattering and thus direct detection. On the other hand, the limits from direct detection for a subdominant DM component are weaker, since the direct detection experiments assume a one-component DM with the observed relic abundance. Therefore, in order to correctly compare with the limits, the produced DM abundance must always be estimated.

Another source of constraints arises from DM annihilations potentially producing an excess of e.g. gamma rays over the galactic background. The most stringent current limits come from the Fermi-LAT satellite experiment [20] constraining the canonical thermal cross section up to ~ 100 GeV DM masses. We focus here on

scenarios with heavier DM candidate and leave further analysis of indirect observables to future work.

A. Quark-induced production

We start by considering the production of the mediator, $\mathcal{M} = \mathcal{S}$, in $q\bar{q}$ annihilation and subsequent decay to DM (as well as the crossed process leading to $\mathcal{D} - N$ scattering), see Figs 1 and 5.

1. Fermionic DM

For fermionic DM, $\mathcal{D} = \chi$, the relevant couplings for a CP-even mediator, \mathcal{S} , are $(y_q^S)^{ij}$ and y_S , see Eq. (1). The former allows the production of \mathcal{S} via a gauge-invariant coupling to SM quarks and the latter its decays to DM. The corresponding Feynman diagram is given in the upper left corner of Fig. 1. At low energies relevant for direct-detection experiments, the mediator can be integrated out leading to the diagram in the upper right corner, which governs $\mathcal{D} - N$ scattering at low momenta. For simplicity, we only consider $(y_u^S)^{11}$, although the analysis can easily be extended to include all quark flavours.

For a CP-odd mediator, $\tilde{\mathcal{S}}$, the couplings above are replaced by the corresponding tilded coefficients in Eq. (3). However, in this case, the tree-level interactions with nuclei are momentum suppressed, and this scenario is out of the reach of current direct detection experiments (and thus LHC cross sections are basically unconstrained). Nevertheless, as discussed in Ref. [21], the future experiments will start probing this scenario as well. Scenarios with CP-odd mediator have also been considered recently in e.g. Refs [22–24]. Here, we concentrate on a CP-even mediator, and leave the phenomenology of CP-odd mediators, utilizing the full strength of the eDMEFT approach, for future work.

The cross section for the DM scattering off nuclei, in terms of eDMEFT couplings, reads [25]

$$\sigma_N = \frac{y_S^2 [(y_u^S)^{11}]^2 (f_N^u)^2 m_N^2 \mu_N^2 v^2}{2\pi \Lambda^2 m_S^4 m_u^2}, \quad (8)$$

where f_N^u is the form factor defined by $\langle N | m_q \bar{q}q | N \rangle \equiv m_N f_N^q$,

$$\mu_N \equiv \frac{m_\chi m_N}{m_\chi + m_N} \quad (9)$$

is the reduced mass of the DM-nucleon system, and $m_N = (m_p + m_n)/2$ is the average nucleon mass.

We calculate the running of the matrix elements $\langle N | y_q^S \bar{q}q | N \rangle$ from the EW scale (where we define our couplings) down to direct-detection energies and the corresponding threshold effects from integrating out the heavy quark flavours following Ref. [26] (see also [27, 28]). For the case with only $(y_u^S)^{11}$ non-zero, this effect is trivial.

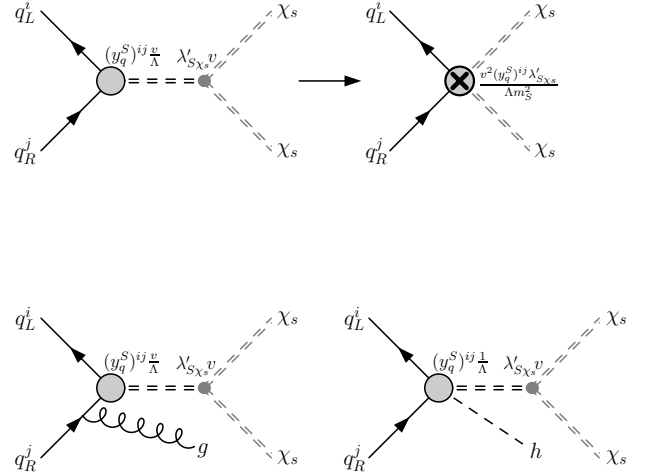


FIG. 5. Relevant diagrams contributing to nuclear interaction with scalar DM (first row) and corresponding DM observables at hadron colliders (monojet and Higgs+ \cancel{E}_T , second row), turning on the interactions $\sim (y_q^S)^{ij}$ and $\sim \lambda'_{S\chi_s}$.

We fix y_S such that we obtain the fraction $f_{\text{rel}} \equiv \Omega_\chi / \Omega_{\text{DM}}$ of the total dark matter abundance. In the direct-detection limits, a single component DM with $f_{\text{rel}} = 1$ is assumed, and thus we require $f_{\text{rel}} \sigma_N \leq \sigma_{\text{X1T}}$ when we compare with the limits for XENON1T.

If $m_\chi < m_S$, the DM annihilation cross section is dominated by the s -channel process to SM quarks via the $D = 5$ operator, and the cross section is thus proportional to $y_S^2 [(y_u^S)^{11}]^2$. This is the same combination appearing in the direct-detection cross section and values avoiding overabundance are disfavoured by experiments (which does not necessarily hold if the DM couples to heavy quarks). Therefore, we concentrate here on the mass range $m_\chi > m_S$, where the dominant annihilation channel is $\chi\chi \rightarrow SS$. The annihilation cross section can thus be estimated (neglecting subleading m_S contributions, which are considered in the numerical results) by [21]

$$\langle \sigma v \rangle (\chi\chi \rightarrow SS) \approx 2.0 \times 10^{-26} \text{ cm}^3 \text{ s}^{-1} y_S^4 \left(\frac{1 \text{ TeV}}{m_\chi} \right)^2, \quad (10)$$

where $v^2 \sim 0.23$. We fix y_S as a function of f_{rel} by comparing this to the standard thermal cross section $\langle \sigma v \rangle_0 = 3 \cdot 10^{-26} \text{ cm}^3 \text{ s}^{-1}$ and using $\Omega h^2 \propto \langle \sigma v \rangle^{-1}$ to scale this with f_{rel} . The latest limit [19] then leads to the bound (see Fig. 6)

$$\frac{|(y_u^S)^{11}|}{\Lambda} \lesssim 2.9 \times 10^{-3} f_{\text{rel}}^{-1/4} \left(\frac{m_S}{1 \text{ TeV}} \right)^2 \text{ TeV}^{-1}. \quad (11)$$

Attaching on the other hand a gluon to the initial state quarks or emitting a Higgs boson—possible directly via the contact interaction $\sim (y_q^S)^{ij}$ —leads to final states

considered in LHC searches for DM, i.e. monojet and Higgs+ \cancel{E}_T signatures. The corresponding diagrams are given in the lower panel of Fig. 1.

We calculate the maximal cross sections for these processes at the LHC at 13 TeV center-of-mass energy using MadGraph [29] and employing the direct-detection limit, Eq. (11), for two benchmark scenarios: ($m_S = 400$ GeV, $m_{\chi_s} = 500$ GeV) and ($m_S = 500$ GeV, $m_{\chi_s} = 1$ TeV). We arrive at (fixing for simplicity $f_{\text{rel}} = 1$)

$$\begin{aligned}\sigma_j|_{m_{\chi_s}=500 \text{ GeV}} &\lesssim 3.0 \cdot 10^{-7} \text{ fb}, \\ \sigma_j|_{m_{\chi_s}=1 \text{ TeV}} &\lesssim 3.5 \cdot 10^{-8} \text{ fb},\end{aligned}\quad (12)$$

and

$$\begin{aligned}\sigma_{h+\cancel{E}_T}|_{m_{\chi_s}=500 \text{ GeV}} &\lesssim 2.0 \cdot 10^{-8} \text{ fb}, \\ \sigma_{h+\cancel{E}_T}|_{m_{\chi_s}=1 \text{ TeV}} &\lesssim 3.4 \cdot 10^{-8} \text{ fb}.\end{aligned}\quad (13)$$

These cross sections are tiny, but serve here as reference values for this utterly simplified scenario with only two additional couplings turned on. For example, already allowing for heavy quark flavors to couple to the mediator, interpolating between the light quark case and the gluon case discussed in the next section, is expected to increase the cross section significantly.

2. Scalar DM

For scalar DM, $\mathcal{D} = \chi_s$, the corresponding couplings are still $(y_q^S)^{ij}$ for the $q\bar{q}$ production of the mediator, while the decay to DM is now induced by the portal term $\lambda'_{S\chi_s}$. The Feynman diagrams for the processes discussed above are analogously presented in Fig. 5, where χ_s is represented by faint dashed double-lines. Note that for a CP-odd mediator the above portal linear in \tilde{S} is not present.

The scattering cross section off nuclei now becomes [25]

$$\sigma_N = \frac{(\lambda'_{S\chi_s})^2 (y_{11}^S)^2 (f_N^u)^2 m_N^2 \mu_N^2 v^4}{16\pi \Lambda^2 m_S^4 m_u^2 m_{\chi_s}^2}. \quad (14)$$

Again, to estimate the relic density, we concentrate on $m_{\chi_s} > m_S$, whence the annihilation cross section yields [21]

$$\begin{aligned}\langle\sigma v\rangle(\chi_s\chi_s \rightarrow SS) &\approx 5.8 \times 10^{-26} \text{ cm}^3 \text{ s}^{-1} \\ &\cdot \left(\frac{\lambda'_{S\chi_s} v}{2\sqrt{2}m_S}\right)^4 \left(\frac{1 \text{ TeV}}{m_{\chi_s}}\right)^2.\end{aligned}\quad (15)$$

Trading $\lambda'_{S\chi_s}$ for f_{rel} similarly as above, we show the bounds from direct detection again in Fig. 6. For the benchmark scenarios ($m_S = 400$ GeV, $m_{\chi_s} = 500$ GeV) and ($m_S = 500$ GeV, $m_{\chi_s} = 1$ TeV), we obtain limits

$$\begin{aligned}\frac{|(y_u^S)^{11}|}{\Lambda}|_{m_{\chi_s}=500 \text{ GeV}} &\lesssim 7.5 \times 10^{-4} f_{\text{rel}}^{-1/4} \text{ TeV}^{-1}, \\ \frac{|(y_u^S)^{11}|}{\Lambda}|_{m_{\chi_s}=1 \text{ TeV}} &\lesssim 1.9 \times 10^{-3} f_{\text{rel}}^{-1/4} \text{ TeV}^{-1}.\end{aligned}\quad (16)$$

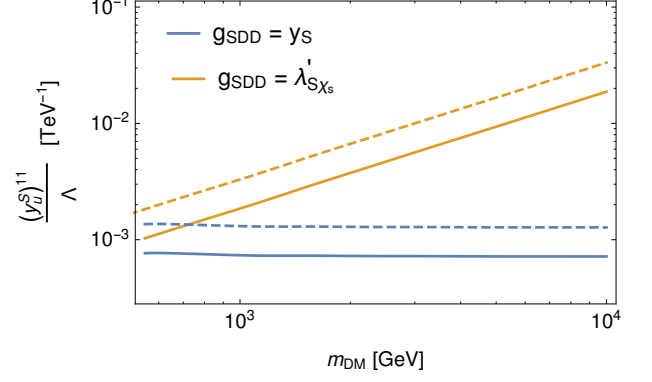


FIG. 6. Limits from the direct-detection experiments for the coupling $(y_u^S)^{11}/\Lambda$ as a function of the DM mass. Blue (yellow) lines correspond to fermionic (scalar) DM with CP-even mediator, and $g_{S\chi\chi}$ denotes the corresponding mediator-DM coupling. In the plot, we have fixed $m_S = 500$ GeV, and the solid (dashed) lines correspond to $f_{\text{rel}} = 1$ ($f_{\text{rel}} = 0.1$).

Using these and fixing $f_{\text{rel}} = 1$, the maximal values of the LHC cross sections become

$$\begin{aligned}\sigma_j|_{m_{\chi_s}=500 \text{ GeV}} &\lesssim 1.2 \cdot 10^{-7} \text{ fb}, \\ \sigma_j|_{m_{\chi_s}=1 \text{ TeV}} &\lesssim 6.8 \cdot 10^{-9} \text{ fb},\end{aligned}\quad (17)$$

and

$$\begin{aligned}\sigma_{h+\cancel{E}_T}|_{m_{\chi_s}=500 \text{ GeV}} &\lesssim 1.6 \cdot 10^{-8} \text{ fb}, \\ \sigma_{h+\cancel{E}_T}|_{m_{\chi_s}=1 \text{ TeV}} &\lesssim 8.1 \cdot 10^{-10} \text{ fb}.\end{aligned}\quad (18)$$

which again are tiny as expected for this simplified scenario.

B. Gluon-fusion production

We now turn to the case of coupling the mediator to a gg state, allowing its production in gluon-gluon fusion, which is complementary to the case of external $q\bar{q}$ states. Since the coupling to the DM is still assumed to be induced by y_S and $\lambda'_{S\chi_s}$, for the cases of fermionic DM χ with a CP-even mediator S and scalar DM χ_s , respectively, we only replace $(y_u^S)^{11}$ by c_G^S to couple the mediator to gluons. The relevant diagrams are given in Figs 2 and 7. Note that, due to the absence of the Higgs contact interaction in the NP sector, the Higgs+ \cancel{E}_T channel is significantly suppressed with respect to the monojet signature, requiring a $G\bar{G}h$ interaction, induced in the SM via a top loop, and we do not consider that here.

1. Fermionic DM

Starting with the SGG interaction at the EW scale will now induce the $\mathcal{S}\bar{q}q$ couplings at the nuclear energy

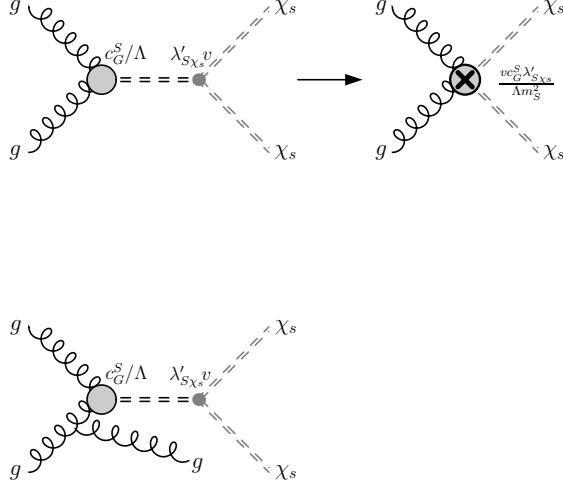


FIG. 7. Relevant diagrams contributing to nuclear interaction with scalar DM (first row) and corresponding DM observables at hadron colliders (monojet, second row), turning on the interactions $\sim c_G^S$ and $\sim \lambda'_{S\chi_s}$.

scale [26]. Therefore, the cross section for scattering off nuclei now becomes

$$\sigma_N = \frac{y_S^2 (c_G^S)^2 m_N^2 \mu_N^2}{\pi \Lambda^2 m_S^4} \left(\sum_{q=u,d,s} (c_G^q f_N^q) + \frac{2}{9} c_G^g f_N^g \right)^2, \quad (19)$$

where c_G^q and c_G^g account for the running and threshold effects down to the nuclear-energy scale, the gluonic form factor is defined as $\langle N | -\frac{g_s^2}{16\pi^2} G_{\mu\nu} G^{\mu\nu} | N \rangle \equiv \frac{2}{9} m_N f_N^g$, and we again employ the results of Ref. [26].

Comparing now with XENON1T results, leads to the bound

$$\frac{c_G^S}{\Lambda} \lesssim 1.3 \times 10^3 f_{\text{rel}}^{-1/4} \left(\frac{m_S}{1 \text{ TeV}} \right)^2 \text{ TeV}^{-1}, \quad (20)$$

shown in Fig. 8.

The monojet cross section is thus constrained for the benchmark scenarios ($m_S = 400 \text{ GeV}, m_{\chi_s} = 500 \text{ GeV}$) and ($m_S = 500 \text{ GeV}, m_{\chi_s} = 1 \text{ TeV}$) and $f_{\text{rel}} = 1$ to

$$\begin{aligned} \sigma_j|_{m_{\chi_s}=500 \text{ GeV}} &\lesssim 1.9 \cdot 10^3 \text{ fb}, \\ \sigma_j|_{m_{\chi_s}=1 \text{ TeV}} &\lesssim 250 \text{ fb}. \end{aligned} \quad (21)$$

These values are significantly higher than in the quark-induced production, connected to the relative growth of the gluon parton distribution functions with respect to the up-quark one from nuclear to collider energies and the negative interference between the quark and gluon form factors at nuclear scales. Therefore this scenario provides an interesting possibility to partially evade the strong direct-detection limits.

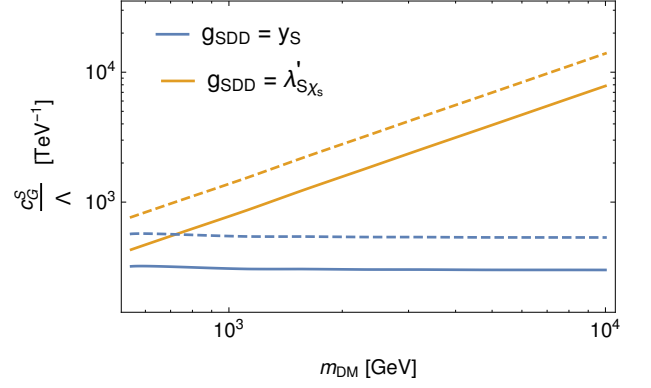


FIG. 8. Limits from the direct-detection experiments for the coupling c_G^S/Λ as a function of the DM mass. Blue (yellow) lines correspond to fermionic (scalar) DM with CP-even mediator, and $g_{S\chi\chi}$ denotes the corresponding mediator–DM coupling. In the plot, we have fixed $m_S = 500 \text{ GeV}$, and the solid (dashed) lines correspond to $f_{\text{rel}} = 1$ ($f_{\text{rel}} = 0.1$).

2. Scalar DM

For scalar DM (with a CP-even mediator), we obtain

$$\sigma_N = \frac{(\lambda'_{S\chi_s})^2 (c_G^S)^2 m_N^2 \mu_N^2 v^2}{8\pi \Lambda^2 m_S^4 m_u^2} \cdot \left(\sum_{q=u,d,s} (c_G^q f_N^q) + \frac{2}{9} c_G^g f_N^g \right)^2, \quad (22)$$

and the resulting bounds are shown in Fig. 8. For the benchmark scenarios ($m_S = 400 \text{ GeV}, m_{\chi_s} = 500 \text{ GeV}$) and ($m_S = 500 \text{ GeV}, m_{\chi_s} = 1 \text{ TeV}$), the limits read

$$\begin{aligned} \frac{c_G^S}{\Lambda} |_{m_{\chi_s}=500 \text{ GeV}} &\lesssim 310 f_{\text{rel}}^{-1/4} \text{ TeV}^{-1}, \\ \frac{c_G^S}{\Lambda} |_{m_{\chi_s}=1 \text{ TeV}} &\lesssim 780 f_{\text{rel}}^{-1/4} \text{ TeV}^{-1}. \end{aligned} \quad (23)$$

In consequence, the monojet cross section is bounded by

$$\begin{aligned} \sigma_j|_{m_{\chi_s}=500 \text{ GeV}} &\lesssim 670 \text{ fb}, \\ \sigma_j|_{m_{\chi_s}=1 \text{ TeV}} &\lesssim 140 \text{ fb}. \end{aligned} \quad (24)$$

Again the cross sections are comparable to the fermionic-DM case, and the conclusion that the gluon-induced production provides an interesting scenario also for collider searches.

C. Higgs–mediator portal

Another interesting option is to couple the DM to the SM via the portal term involving the mediator and the

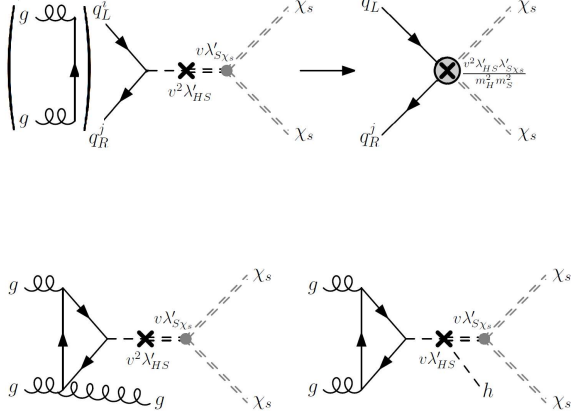


FIG. 9. Relevant diagrams contributing to nuclear interaction with scalar DM (first row) and corresponding DM observables at hadron colliders (monojet and Higgs+ E_T , second row), turning on the interactions $\sim \lambda'_{HS}$ and $\sim \lambda'_{S\chi_s}$.

Higgs field, $\sim \lambda'_{HS}$, turning on this coupling in addition to y_S ($\lambda'_{S\chi_s}$) for fermionic (scalar) DM. This allows for a SM-like production of the scalar mediator via its mixing with the Higgs field, while its coupling to the DM remains as in the cases discussed above. The relevant diagrams are given in Figs 3 and 9. Note that in the figures for simplicity, we employ a mass-insertion approximation, where the mixing of the Higgs with the new scalar is treated as an interaction, marked by a black cross. In the numerical analysis below, we instead diagonalize the $H - S$ system.

Moreover, the Higgs+ E_T channel receives the contribution from the second Higgs field present in the portal, as depicted by the lower-right diagrams in Figs 3 and 9, respectively.

We diagonalise the Higgs- S system via a rotation

$$\begin{aligned} h^0 &= h \cos \alpha + S \sin \alpha, \\ H^0 &= -h \sin \alpha + S \cos \alpha, \end{aligned} \quad (25)$$

with the angle, α , given by

$$\tan 2\alpha = \frac{2\lambda'_{HS}v^2}{2\lambda_H v^2 - \mu_S^2}. \quad (26)$$

Further, we trade λ_H (the coefficient of the quartic Higgs operator) and μ_S^2 for the masses of the eigenstates, m_h and m_H , the lighter of which we identify with the 125-GeV Higgs boson.

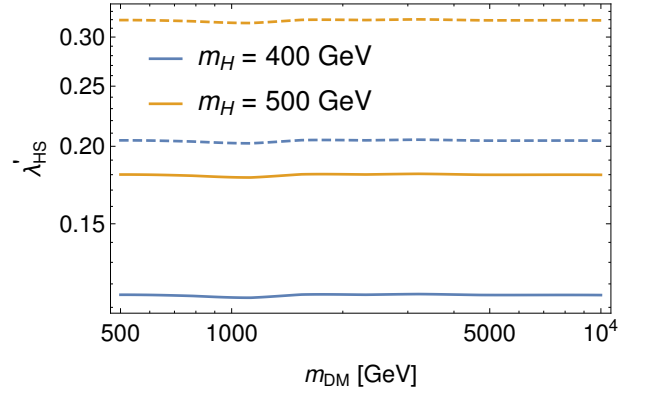


FIG. 10. Limits from the direct-detection experiments for the coupling λ'_{HS} as a function of the DM mass for the Higgs-mediator portal scenario with fermionic DM. Blue (yellow) lines correspond to a mass of the heavy scalar eigenstate of 400 GeV (500 GeV). Solid (dashed) lines correspond to $f_{\text{rel}} = 1$ ($f_{\text{rel}} = 0.1$).

1. Fermionic DM

For fermionic DM, we finally obtain

$$\begin{aligned} \sigma_N &= \frac{y_S^2 f_N^2 m_N^2 \mu_N^2}{\pi v^2} \sin^2 \alpha \cos^2 \alpha \left(\frac{1}{m_h^2} - \frac{1}{m_H^2} \right)^2 \\ &= \frac{y_S^2 f_N^2 m_N^2 \mu_N^2 (\lambda'_{HS})^2 v^2}{\pi m_h^4 m_H^4}. \end{aligned} \quad (27)$$

For the relic density calculation, we now add the $\bar{t}t$ channel mediated by the Higgs doublet. We focus on $m_\chi > m_t$ and use the estimate [21]

$$\begin{aligned} \langle \sigma v \rangle (\bar{\chi}\chi \rightarrow \bar{t}t) &\approx 4.0 \times 10^{-26} \text{ cm}^3 \text{ s}^{-1} \\ &\cdot y_S^2 \sin^2 \alpha \cos^2 \alpha \left(\frac{1 \text{ TeV}}{m_\chi} \right)^2. \end{aligned} \quad (28)$$

For the scalar channels, we use Eq. (10) after scaling the couplings with the appropriate mixing coefficients given in Eq. (25).

Comparing now with XENON1T results, leads to the bounds shown in Fig. 10, and the monojet cross section is bounded due to the direct detection limit as

$$\begin{aligned} \sigma_j|_{m_\chi=500 \text{ GeV}} &\lesssim 1.1 \cdot 10^{-3} \text{ fb}, \\ \sigma_j|_{m_\chi=1 \text{ TeV}} &\lesssim 3.3 \cdot 10^{-4} \text{ fb}. \end{aligned} \quad (29)$$

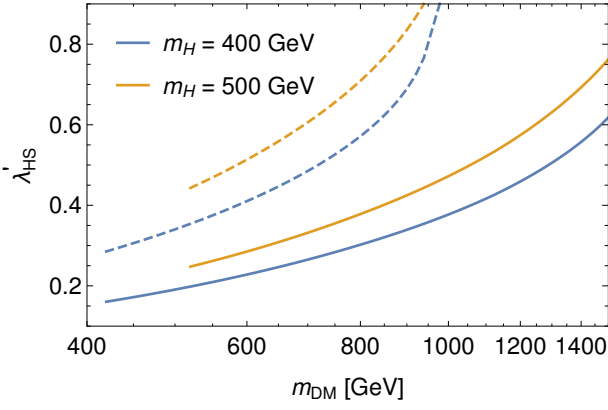


FIG. 11. Limits from the direct-detection experiments for the coupling λ'_{HS} as a function of the DM mass for the Higgs–mediator portal scenario with scalar DM. Blue (yellow) lines correspond to a mass of the heavy scalar eigenstate of 400 GeV (500 GeV). Solid (dashed) lines correspond to $f_{\text{rel}} = 1$ ($f_{\text{rel}} = 0.1$).

2. Scalar DM

For scalar DM, we arrive at

$$\begin{aligned} \sigma_N &= \frac{(\lambda'_{S\chi})^2 f_N^2 m_N^2 \mu_N^2}{8\pi m_{\chi_s}^2} \sin^2 \alpha \cos^2 \alpha \left(\frac{1}{m_h^2} - \frac{1}{m_H^2} \right)^2 \\ &= \frac{(\lambda'_{S\chi_s})^2 f_N^2 m_N^2 \mu_N^2 (\lambda'_{HS})^2 v^4}{8\pi m_{\chi_s}^2 m_h^4 m_H^4}. \end{aligned} \quad (30)$$

The annihilation cross section to top quarks for $m_{\chi_s} > m_t$ now becomes [21]

$$\begin{aligned} \langle \sigma v \rangle (\chi_s \chi_s \rightarrow \bar{t}t) &\approx 2.6 \times 10^{-27} \text{ cm}^3 \text{ s}^{-1} \\ &\cdot \lambda_{S\chi_s}^{\prime 2} \sin^2 \alpha \cos^2 \alpha \left(\frac{1 \text{ TeV}}{m_{\chi_s}} \right)^4, \end{aligned} \quad (31)$$

and for the scalar channels we use Eq. (15) scaling the couplings with the mixing coefficients, see Eq. (25). The direct detection bounds are shown in Fig. 11, and the corresponding LHC cross sections are now predicted to be below

$$\begin{aligned} \sigma_j|_{m_{\chi_s}=500 \text{ GeV}} &\lesssim 4.3 \cdot 10^{-4} \text{ fb}, \\ \sigma_j|_{m_{\chi_s}=1 \text{ TeV}} &\lesssim 1.7 \cdot 10^{-4} \text{ fb}. \end{aligned} \quad (32)$$

Although this process is not observable in this restricted scenario, the portal contribution could become relevant in a combined analysis with more operators turned on.

D. Higgs–DM portal

Finally, the DM could also be coupled *directly* to the SM via the Higgs–DM portal, promoting the SM-like

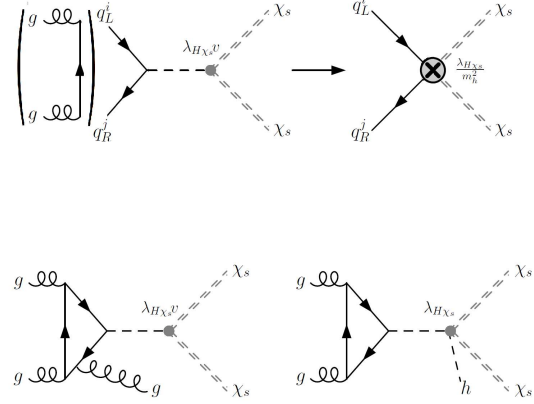


FIG. 12. Relevant diagrams contributing to nuclear interaction with scalar DM (first row) and corresponding DM observables at hadron colliders (monojet and Higgs+ \cancel{E}_T , second row), turning on the interaction $\sim \lambda_{H\chi_s}$.

Higgs boson itself to a mediator to the DM sector, simply by turning on the $D = 5$ operator $\sim y_H^{(2)}$ or $D = 4$ portal $\sim \lambda_{H\chi_s}$, for fermionic or scalar DM, respectively. This corresponds to the traditional SM+singlet DM model studied extensively in the literature; see e.g. Refs [25, 30–33].

While the invisible width of the Higgs boson significantly constrains these operators in case the DM is light, $m_{\chi(s)} < m_h/2$ (see below), for heavier DM they might play an important role in DM production. The corresponding Feynman diagrams for the processes at hand are given in Figs 4 and 12. Again, the Higgs+ \cancel{E}_T channel is induced at leading order via the second Higgs field required by gauge invariance, see the lower-right diagrams.

1. Fermionic DM

For fermionic DM, we obtain the direct detection cross section

$$\sigma_N = \frac{(y_H^{(2)})^2 f_N^2 m_N^2 \mu_N^2}{\pi \Lambda^2 m_h^4}. \quad (33)$$

We trade $y_H^{(2)}/\Lambda$ for f_{rel} from the thermal $\bar{\chi}\chi \rightarrow \bar{t}t, WW, ZZ, hh$ cross section for fixed m_{χ_s} . The dominant contribution corresponds to the t -channel annihilation to hh , which can be obtained using Eq. (10) with substitution $y_S \rightarrow y_H^{(2)} v/\Lambda$. We show the direct detection limits in the $(m_{\text{DM}}, f_{\text{rel}})$ plane in Fig. 13. The monojet cross section is in turn limited to

$$\begin{aligned} \sigma_j|_{m_{\chi_s}=500 \text{ GeV}} &\lesssim 49 \text{ fb}, \\ \sigma_j|_{m_{\chi_s}=1 \text{ TeV}} &\lesssim 3.3 \text{ fb}. \end{aligned} \quad (34)$$

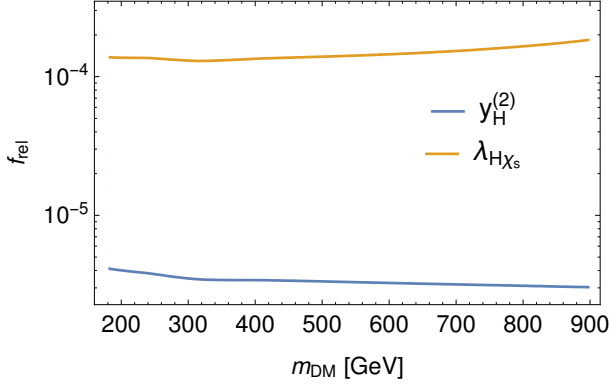


FIG. 13. The blue (yellow) curve shows the maximum allowed fraction of the DM abundance, f_{rel} , as a function of the DM mass fixed by limits from direct detection for the Higgs–DM portal scenario with fermionic (scalar) DM. We only show the mass range $m_{\text{DM}} \lesssim 900$ GeV where the relic abundance is reproduced for $\lambda_{H\chi_s} < 4\pi$.

This scenario could provide another interesting probe for the collider experiments, but is constrained to deliver only a tiny fraction of the DM relic abundance.

2. Scalar DM

For the thermal cross section, including $\chi_s \chi_s \rightarrow \bar{t}t, WW, ZZ, hh$, we use the result from [34]:

$$\begin{aligned} \langle \sigma v \rangle = & \frac{\lambda_{H\chi_s}^2}{2\pi m_{\chi_s}^2 (4 - r_h)^2} \left[6r_t(1 - r_t)^{3/2} \right. \\ & + \sum_{V=W,Z} \delta_V r_V^2 (2 + (1 - 2/r_V)^2) \sqrt{1 - r_V} \\ & \left. + 2 \left(\frac{2\lambda_{H\chi_s}}{\lambda_H} \frac{(1 - r_h/4)r_h}{r_h - 2} + 1 + \frac{r_h}{2} \right)^2 \sqrt{1 - r_h} \right], \end{aligned} \quad (35)$$

where $r_i = m_i^2/m_{\chi_s}^2$, and $\delta_W = 1, \delta_Z = 1/2$.

The direct detection cross section now reads

$$\sigma_N = \frac{\lambda_{H\chi_s}^2 \mu_N^2 m_N^2 f_N^2}{\pi m_{\chi_s}^2 m_h^4}, \quad (36)$$

so we plot the direct detection limits in the $(m_{\text{DM}}, f_{\text{rel}})$ plane in Fig. 13. The LHC cross section in that final case is thus constrained to

$$\sigma_j|_{m_{\chi_s}=500 \text{ GeV}} \lesssim 0.38 \text{ fb}. \quad (37)$$

We note that the cross section is somewhat smaller than that of the fermionic-DM case, making the latter scenario more promising for the collider experiments.

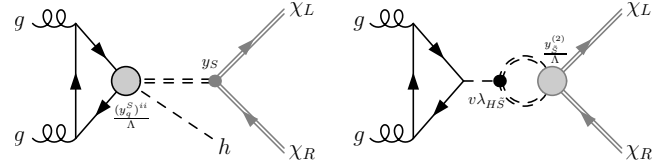


FIG. 14. Potentially important loop diagrams contributing to DM interactions in the eDMEFT, turning on the operators $\sim (y_q^S)^{ij}$ and $\sim y_S$, or $\sim \lambda_{H\tilde{S}}$ and $\sim y_{\tilde{S}}^{(2)}$, respectively. The right diagram involves the quartic portal term $\sim \lambda_{H\tilde{S}}$, which is basically the only relevant term that allows to produce scalar DM via a (pair-produced) pseudo-scalar mediator at the $D \leq 5$ level (via a similar diagrams with $y_{\tilde{S}}^{(2)}/\Lambda \rightarrow \lambda_{\tilde{S}\chi_s}$). See text for details.

E. Further Processes

While dedicated analyses are left for future work, here we already comment on further potentially interesting applications of the eDMEFT framework ranging from the inclusion of loop processes in the EFT, over new production mechanisms, up to analyses of invisible Higgs decays, Higgs pair production and collider searches for the mediator.

1. Loop mediated processes in eDMEFT

While the only loop diagrams we encountered so far contained the SM-like GGh triangle, loops involving $D = 5$ vertices allow for interesting new means to couple the DM to hadrons. First of all, the Yukawa-like operator $\sim (y_q^S)^{ij}$ can now be inserted coming with the top quark ($q = u; ij = 33$) and coupling the mediator to a gluon pair via a (top-)quark loop, see the left diagram in Fig. 14. This operator is expected to be sizable, featuring no (minimal-flavour-violation-like) flavour suppression. The loop suppression is thus lifted by the expected enhancement with m_t/m_q , since the operator is basically unconstrained for the top. A detailed study of flavour constraints on the coefficients, combining them with complementary bounds from limits on the invisible Higgs width and other searches, such as to derive conclusive limits on DM production in the eDMEFT, will be presented elsewhere.

Finally, at the two-loop level, DM production via a portal to a *pseudo-scalar* mediator becomes possible, see the right diagram in Fig. 14. Applied to the case of scalar DM (i.e. replacing $y_{\tilde{S}}^{(2)}/\Lambda \rightarrow \lambda_{\tilde{S}\chi_s}$), this opens the possibility to obtain potentially viable models with a CP-odd mediator.

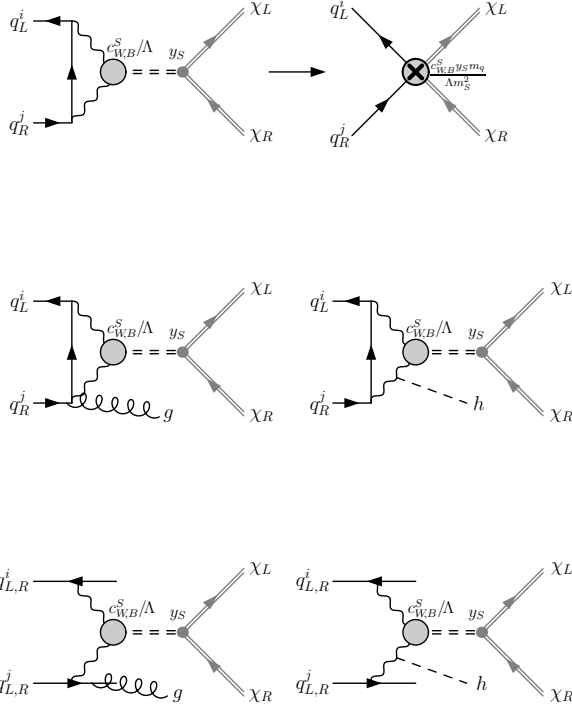


FIG. 15. Diagrams contributing to nuclear interaction with fermionic DM (first row) and DM observables at hadron colliders, turning on the interactions $\sim c_W^S$ and $\sim y_S$. The diagrams are similar for pseudo-scalar mediators, employing the corresponding tilded coefficients, as discussed before. See text for details.

2. Weak-boson fusion

In the same context, a production of the mediator in weak-boson fusion, as depicted by the last two diagrams in Figs 15 and 16, is interesting regarding ‘monojet’ and Higgs+ \cancel{E}_T signals. In fact, if the corresponding $D = 5$ operators feature a sizable coupling $c_{W,B}^S$ (or $S \rightarrow \tilde{S}$, for a CP-odd mediator), DM signals at the LHC can be significant, while limits from direct-detection experiments are met, since the corresponding processes with external quark bi-linears are suppressed by a quark-mass insertion (and a loop factor), see the first (and second) row of Figs 15 and 16.

3. Higgs pair + \cancel{E}_T

Exploring the production of Higgs pairs in association with missing energy could be an additional interesting probe of dark sectors. Indeed, several operators in the eDMEFT allow the production of Higgs pairs along with DM and can be tested in this process. Fig. 17 shows sample diagrams that become potentially important in case the bi-quadratic portal $\sim \lambda_{HS}$ is weak. Beyond the usual case of the mediator decaying to the DM, they also con-

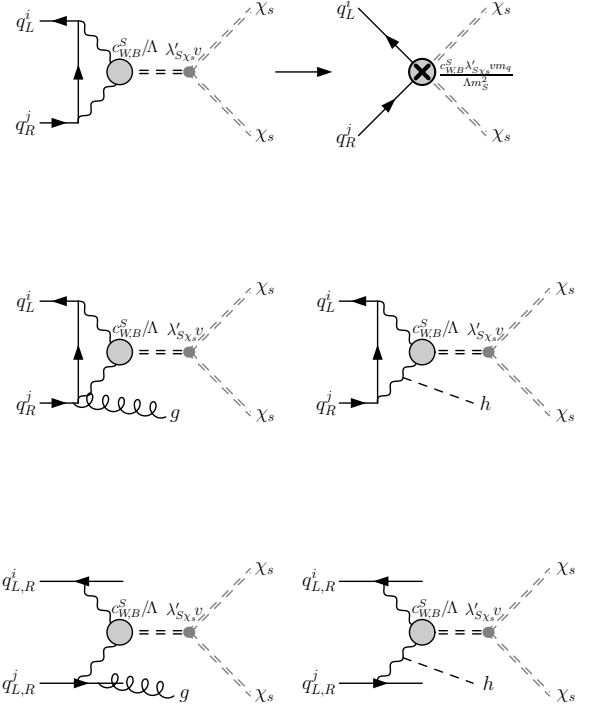


FIG. 16. Diagrams contributing to nuclear interaction with scalar DM (first row) and DM observables at hadron colliders, turning on the interactions $\sim c_W^S$ and $\sim \lambda'_{S\chi_s}$. See text for details.

tain potentially resonant decays of \mathcal{M} to a Higgs pair, after emission of a DM pair, which could allow to see a peak in the hh invariant mass spectrum and boosted Higgs bosons [35]⁵. Although the cross sections are not expected to be large, non-negligible NP couplings could still feature interesting effects in $hh + \cancel{E}_T$ production. A dedicated analysis is needed to examine the actual prospects of this process in the light of the expected limited number of events.

4. Invisible Higgs decays

Note that the eDMEFT can also significantly effect single Higgs physics. For example, for light DM ($m_{\mathcal{D}} \leq m_h$) the eDMEFT operators involving the Higgs field (including $D = 4$ Higgs portals) are constrained more and more severely from limits on invisible Higgs decays. Corresponding diagrams, involving the portal coupling λ'_{HS} together with y_S or $\lambda'_{S\chi_s}$ for the decay to DM are given in the right-hand side of Fig. 18, while those with direct

⁵ Note that, for the given couplings turned on, there are additional (potentially) similar important contributions, attaching the Higgs or mediator lines differently in the diagrams above (including Higgs emissions from SM lines).

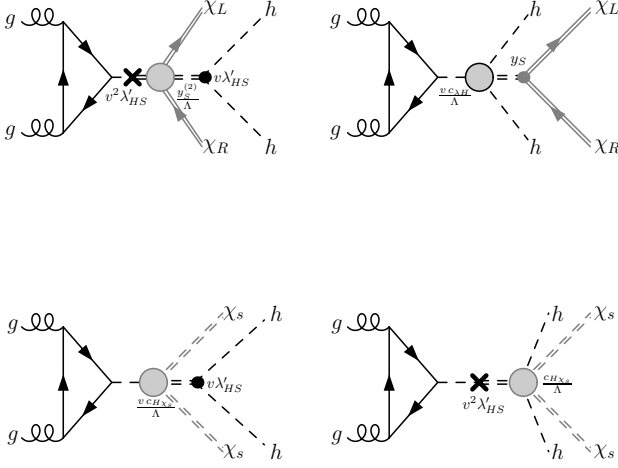


FIG. 17. Selected diagrams contributing to Higgs pair production in association with E_T , turning on the interactions $\sim \lambda'_{HS}, y_S^{(2)}$ or $\sim c_{\lambda H}, y_S$ in the case of fermionic DM (first row) and $\sim \lambda'_{HS}, c_{H\chi_s}$ in the case of scalar DM (second row). See text for details.

$h-D-D$ interactions $y_H^{(2)}$ or $\lambda_{H\chi_s}$ are depicted in the left-hand side of the same figure. A production of the mediator via $D = 5$ eDMEFT operators avoiding these constraints becomes particularly interesting.

Moreover, the additional scalar particle \mathcal{S} can have an interesting impact on the nature of the electroweak phase transition, which in the SM is not first order, such as to allow for electroweak baryogenesis [36, 37]. With the help of a light \mathcal{S} , electroweak baryogenesis can become viable (see, e.g. [38–41]). In turn, the DM phenomenology will be affected. Including such a scenario in our framework is also left for the future.

5. \mathcal{S} Resonance search

Finally, one can also search directly for the mediator by looking for a resonant enhancement in the di-jet, $t\bar{t}$, di-lepton, or di-boson spectrum. These processes can also be described consistently in the eDMEFT, since the inclusion of the mediator as a dynamical degree of freedom is a defining feature of the setup, and their study can deliver important insight on the nature of DM. Sample diagrams for the first two processes, involving the couplings λ'_{HS} and $(y_q^S)^{ij}$ are shown in Fig. 19, and the other resonant processes are generated via similar diagrams (including the production of the resonance in gluon fusion and the decay via Higgs mixing). Again, the black cross denotes a mass insertion, while in the (diagonal) mass basis just the heavy mediator is exchanged in the s-channel, with its coupling to the $t\bar{t}$ state governed by the Higgs admixture. Resonance searches are in fact a powerful complementary tool to understand dark sectors and to probe the coupling structure of the mediator even in the case

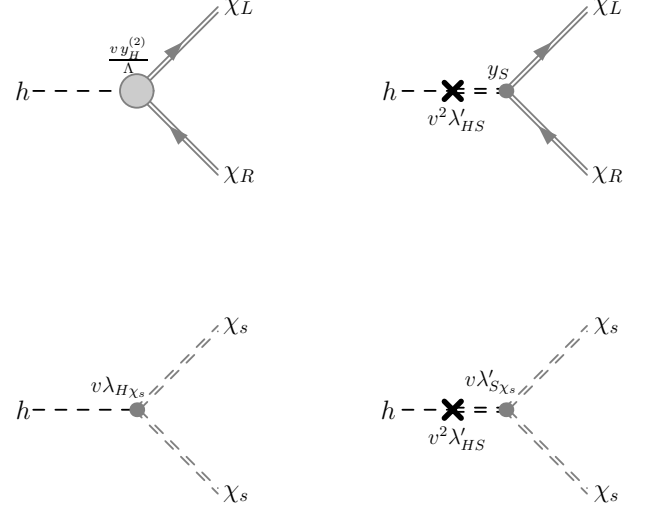


FIG. 18. Contributions to the invisible width of the Higgs boson from turning on the interactions $\sim y_H^{(2)}$, $\sim \lambda'_{HS}, y_S$, $\sim \lambda_{H\chi_s}$, $\sim \lambda'_{HS}, \lambda'_{S\chi_s}$.

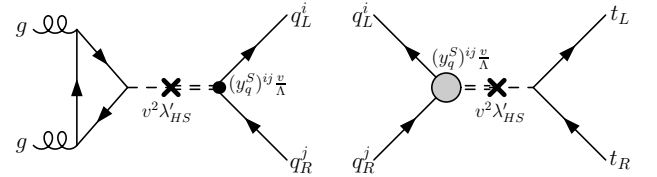


FIG. 19. Resonant contributions of the mediator to di-jet and $t\bar{t}$ final states, turning on the interactions $\sim \lambda'_{HS}$ and $\sim (y_q^S)^{ij}$. Replacing the latter by $c_{W,B,G}^S$ or $(y_\ell^S)^{ij}$ leads to further interesting contributions to di-boson, di-jet, and di-lepton final states.

where its production is dominated by a single operator. Being able to combine this information with that of the other DM observables in a single consistent, yet general, framework is a particular strength of the eDMEFT.

III. CONCLUSIONS

We have presented a new framework to describe DM phenomenology, which can be used to consistently confront limits from direct-detection experiments and the relic abundance with possible collider signatures at high energies, while maintaining a high degree of model-independence. Both the DM and mediator fields remain as propagating degrees of freedom, whereas additional new physics is described in the form of higher-dimensional operators. As an application of the framework, focusing on the level of $D = 5$ operators, we derived possible cross sections in monojet and Higgs+ E_{miss} signatures at the LHC. Considering the limits from di-

rect detection and reproducing (a certain fraction of) the DM relic density, for scalar mediator, we found that the most promising case for the collider searches is gluon induced production, which could lead to sizable LHC cross sections both for fermionic and scalar DM. Cases with pseudoscalar mediators are still rather unconstrained by direct-detection experiments, and eDMEFT will reveal its full strength with the future generation of direct-detection experiments. These results are valid in a more general context than those derived in conventional (simplified) models. A plethora of possible further applications of the framework is left for future work.

ACKNOWLEDGMENTS

We are grateful to Giorgio Arcadi, Martin Bauer, Fari-naldo Queiroz, Valentin Tenorth, and Stefan Vogel for useful discussions and comments.

-
- [1] S. Bruggisser, F. Riva, and A. Urbano, JHEP **11**, 069 (2016), arXiv:1607.02475 [hep-ph].
 - [2] G. Busoni, A. De Simone, E. Morgante, and A. Riotto, Phys. Lett. **B728**, 412 (2014), arXiv:1307.2253 [hep-ph].
 - [3] M. Bauer, A. Butter, N. Desai, J. Gonzalez-Fraile, and T. Plehn, Phys. Rev. **D95**, 075036 (2017), arXiv:1611.09908 [hep-ph].
 - [4] A. Carmona, F. Goertz, and A. Papaefstathiou, Phys. Rev. **D95**, 095022 (2017), arXiv:1606.02716 [hep-ph].
 - [5] R. Franceschini, G. F. Giudice, J. F. Kamenik, M. McCullough, F. Riva, A. Strumia, and R. Torre, JHEP **07**, 150 (2016), arXiv:1604.06446 [hep-ph].
 - [6] B. Gripaios and D. Sutherland, JHEP **08**, 103 (2016), arXiv:1604.07365 [hep-ph].
 - [7] M. A. Luty, Phys. Rev. **D57**, 1531 (1998), arXiv:hep-ph/9706235 [hep-ph].
 - [8] A. G. Cohen, D. B. Kaplan, and A. E. Nelson, Phys. Lett. **B412**, 301 (1997), arXiv:hep-ph/9706275 [hep-ph].
 - [9] G. F. Giudice, C. Grojean, A. Pomarol, and R. Rattazzi, JHEP **06**, 045 (2007), arXiv:hep-ph/0703164 [hep-ph].
 - [10] M. Chala, G. Durieux, C. Grojean, L. de Lima, and O. Matsedonskyi, JHEP **06**, 088 (2017), arXiv:1703.10624 [hep-ph].
 - [11] F. Goertz, (2017), arXiv:1711.03162 [hep-ph].
 - [12] M. Beltran, D. Hooper, E. W. Kolb, Z. A. C. Krusberg, and T. M. P. Tait, JHEP **09**, 037 (2010), arXiv:1002.4137 [hep-ph].
 - [13] Y. Bai, P. J. Fox, and R. Harnik, JHEP **12**, 048 (2010), arXiv:1005.3797 [hep-ph].
 - [14] J. Goodman, M. Ibe, A. Rajaraman, W. Shepherd, T. M. P. Tait, and H.-B. Yu, Phys. Rev. **D82**, 116010 (2010), arXiv:1008.1783 [hep-ph].
 - [15] A. Rajaraman, W. Shepherd, T. M. P. Tait, and A. M. Wijangco, Phys. Rev. **D84**, 095013 (2011), arXiv:1108.1196 [hep-ph].
 - [16] F. Goertz, Phys. Rev. Lett. **113**, 261803 (2014), arXiv:1406.0102 [hep-ph].
 - [17] C. Boehm, M. J. Dolan, C. McCabe, M. Spannowsky, and C. J. Wallace, JCAP **1405**, 009 (2014), arXiv:1401.6458 [hep-ph].
 - [18] C. Arina, E. Del Nobile, and P. Panci, Phys. Rev. Lett. **114**, 011301 (2015), arXiv:1406.5542 [hep-ph].
 - [19] E. Aprile et al. (XENON), Phys. Rev. Lett. **119**, 181301 (2017), arXiv:1705.06655 [astro-ph.CO].
 - [20] M. Ackermann et al. (Fermi-LAT), Phys. Rev. Lett. **115**, 231301 (2015), arXiv:1503.02641 [astro-ph.HE].
 - [21] G. Arcadi, M. Dutra, P. Ghosh, M. Lindner, Y. Mambrini, M. Pierre, S. Profumo, and F. S. Queiroz, (2017), arXiv:1703.07364 [hep-ph].
 - [22] Y. Mambrini, G. Arcadi, and A. Djouadi, Phys. Lett. **B755**, 426 (2016), arXiv:1512.04913 [hep-ph].
 - [23] G. Arcadi, M. Lindner, F. S. Queiroz, W. Rodejohann, and S. Vogl, (2017), arXiv:1711.02110 [hep-ph].
 - [24] M. Bauer, M. Klassen, and V. Tenorth, (2017), arXiv:1712.06597 [hep-ph].
 - [25] T. Alanne, K. Tuominen, and V. Vaskonen, Nucl. Phys. **B889**, 692 (2014), arXiv:1407.0688 [hep-ph].
 - [26] R. J. Hill and M. P. Solon, Phys. Rev. **D91**, 043505 (2015), arXiv:1409.8290 [hep-ph].
 - [27] F. Bishara, J. Brod, B. Grinstein, and J. Zupan, JHEP **11**, 059 (2017), arXiv:1707.06998 [hep-ph].
 - [28] F. Bishara, J. Brod, B. Grinstein, and J. Zupan, (2017), arXiv:1708.02678 [hep-ph].
 - [29] J. Alwall, R. Frederix, S. Frixione, V. Hirschi, F. Maltoni, O. Mattelaer, H. S. Shao, T. Stelzer, P. Torrielli, and M. Zaro, JHEP **07**, 079 (2014), arXiv:1405.0301 [hep-ph].
 - [30] J. McDonald, Phys. Rev. **D50**, 3637 (1994), arXiv:hep-ph/0702143 [HEP-PH].
 - [31] C. P. Burgess, M. Pospelov, and T. ter Veldhuis, Nucl. Phys. **B619**, 709 (2001), arXiv:hep-ph/0011335 [hep-ph].
 - [32] J. M. Cline, K. Kainulainen, P. Scott, and C. Weniger, Phys. Rev. **D88**, 055025 (2013), [Erratum: Phys. Rev. **D92**, no.3, 039906(2015)], arXiv:1306.4710 [hep-ph].
 - [33] L. Lopez-Honorez, T. Schwetz, and J. Zupan, Phys. Lett. **B716**, 179 (2012), arXiv:1203.2064 [hep-ph].
 - [34] J. M. Cline and K. Kainulainen, JCAP **1301**, 012 (2013), arXiv:1210.4196 [hep-ph].
 - [35] Z. Kang, P. Ko, and J. Li, Phys. Rev. Lett. **116**, 131801 (2016), arXiv:1504.04128 [hep-ph].
 - [36] K. Kajantie, M. Laine, K. Rummukainen, and M. E. Shaposhnikov, Phys. Rev. Lett. **77**, 2887 (1996), arXiv:hep-ph/9605288 [hep-ph].
 - [37] K. Rummukainen, M. Tsypin, K. Kajantie, M. Laine, and M. E. Shaposhnikov, Nucl. Phys. **B532**, 283 (1998), arXiv:hep-lat/9805013 [hep-lat].
 - [38] G. W. Anderson and L. J. Hall, Phys. Rev. **D45**, 2685 (1992).
 - [39] J. R. Espinosa and M. Quiros, Phys. Lett. **B305**, 98 (1993), arXiv:hep-ph/9301285 [hep-ph].
 - [40] J. Choi and R. R. Volkas, Phys. Lett. **B317**, 385 (1993), arXiv:hep-ph/9308234 [hep-ph].
 - [41] J. McDonald, Phys. Lett. **B323**, 339 (1994).